Morphological models of complex ordered materials based on inhomogeneously clipped Gaussian fields

Cedric J. Gommes[1,2] and Jean-Paul Pirard[1]
[1]*Department of Chemical Engineering, University of Liège, Allée du 6 Août 3, B-4000 Liège, Belgium*
[2]*Department of Inorganic Chemistry and Catalysis, Utrecht University, Sorbonnelaan 16, 3584 CA Utrecht, The Netherlands*
(Received 25 June 2009; published 8 December 2009)

Clipping a Gaussian random field at a level that is position-dependent yields statistically inhomogeneous morphologies, relevant to many ordered nanostructured materials. The one-point and two-point probability functions of the morphology are derived, as well as a general relation between the specific surface area and the gradient of the clipping function. The general results are particularized for the comprehensive analysis of small-angle x-ray scattering and nitrogen adsorption of SBA-15 ordered mesoporous silica.

DOI: 10.1103/PhysRevE.80.061401 PACS number(s): 61.43.Hv, 81.07.−b, 61.43.Bn, 68.49.−h

Morphological models are needed for the quantitative characterization of the microstructure of materials, and for the understanding of their structure-dependent properties [1–5]. The main difficulty when developing such models is to find a balance between conceptual simplicity and realism. The former is indispensable for the reliable analysis of characterization data with as few parameters as possible. The latter implies that as many morphological features as possible be incorporated in the materials description, which often entails some type of randomness. Stochastic models based on Gaussian random fields offer a way through these almost antagonistic requirements [6–10].

A Gaussian random field (GRF) $w(\mathbf{x})$ is a stochastic function of space having mean 0 and variance 1, and characterized by its correlation function $g(r)=\langle w(\mathbf{r})w(\mathbf{0})\rangle$. As initially proposed by Cahn in the context of spinodal decomposition [6], the morphology of a material can be modeled by defining one phase as the locus of all points where a GRF takes values larger than a clipping constant α. Figures 1(a) and 1(b) show a realization of a GRF having $g(r)=1/\cosh(r/\xi)$ with $\xi=4$ nm, and the clipped morphology with $\alpha=0$. Models based on clipped GRFs have proved useful for analyzing the morphology of a wide variety of amorphous materials, from polymer blends [11] to foodstuff [12], among others [13]. More elaborate models, based on two clipping constants, have been used to characterize microemulsions [8,9]. Combining two statistically independent GRFs further enables to model filamentary morphologies [14] and notably gels [15]. Other developments with Gaussian fields concern notably the three-dimensional (3D) reconstruction of materials from their two-dimensional (2D) imaging [16], the advanced estimation of the models parameters [17–19], as well as with the generalization of the concept to Poisson fields [20].

All the mentioned models and methods are applicable to disordered morphologies having short-ranged correlation. Progress in the chemistry of materials, however, led to the development of hosts of ordered materials, the morphology of which cannot be analyzed with the existing models. These materials notably encompass colloidal crystals [21], as well as the large family of ordered mesoporous materials synthesized by liquid crystal templating [22], many of which have long-ranged correlations. Their thorough characterization requires statistically inhomogeneous morphological models, which have received remarkably little attention so far [23].

In the present paper, we propose a family of morphological models, obtained by clipping a GRF $w(\mathbf{x})$ at a level $\alpha(\mathbf{x})$ that is a deterministic function of space. The indicator function—taking the value 1 in a given phase and 0 in the other—is formally defined as $f(\mathbf{x})=\Theta[w(\mathbf{x})-\alpha(\mathbf{x})]$, where Θ is the step function. A wide variety of morphologies can be modeled according to the chosen clipping function $\alpha(\mathbf{x})$. Figure 1(c) was obtained with $\alpha(\mathbf{x})$ being a linear function of one space coordinate, which provides a model of rough interfaces. Other examples of inhomogeneously clipped Gaussian fields are given in Fig. 2. Globular objects with complex morphologies are modeled with $\alpha(\mathbf{x})$ being a radial function [Figs. 2(a) and 2(c)]. Disordered lamellar structures can be modeled with $\alpha(\mathbf{x})$ being a periodic function [Fig. 2(b)]. As a last example, a structure reminiscent of an astronomical object is modeled in Fig. 2(d) based on an axisymmetric clipping function.

Many measurable properties of materials can be expressed through their n-point probability functions [1,2]. Volumes are related to the one-point probability function $S_1(\mathbf{x})$, defined as the probability that point $\mathbf{x}$ belongs to the phase. In the context of a clipped GRF model, S_1 is equal to the probability that $w(\mathbf{x})$ takes locally a value larger than $\alpha(\mathbf{x})$, namely,

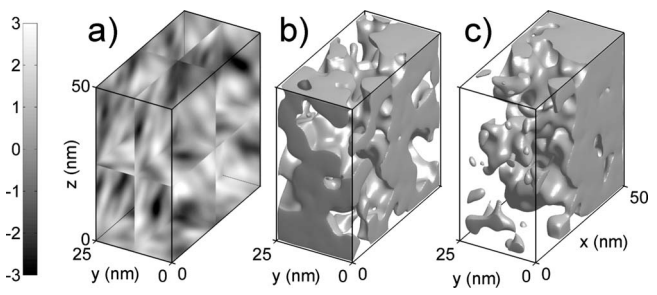

FIG. 1. Realization of a Gaussian random field with $\xi=4$ nm (a), and the morphologies obtained by clipping the realization with $\alpha=0$ (b), and $\alpha=(25-x)/5$(c).

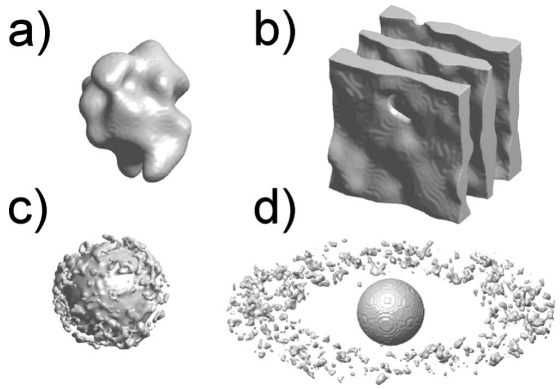

FIG. 2. Example of morphologies that can be obtained by clipping a Gaussian field with a monotonous radial function (a), with a periodic function (b), with a nonmonotonous radial function (c), and with a function having axial symmetry (d).

$$S_1(\mathbf{x}) = \frac{1}{2} - \frac{1}{2}\mathrm{erf}\left(\frac{\alpha(\mathbf{x})}{\sqrt{2}}\right), \tag{1}$$

which results from $w(\mathbf{x})$ being Gaussian distributed; erf is the error function. Contrary to statistically homogeneous models, S_1 is here position-dependent; the average volume of a phase, e.g., of the objects in Fig. 2, is the integral of $S_1(\mathbf{x})$ over space.

Specific surface areas and small-angle scattering patterns depend on the two-point probability function $S(\mathbf{x}_1,\mathbf{x}_2)$ of the material. The latter is the probability that points $\mathbf{x}_1$ and $\mathbf{x}_2$ both belong to a given phase. This is estimated as the probability that $w(\mathbf{x}_1)$ and $w(\mathbf{x}_2)$ be both larger than $\alpha(\mathbf{x}_1)$ and $\alpha(\mathbf{x}_2)$, namely,

$$S_2(\mathbf{x}_1,\mathbf{x}_2) = S_1(\mathbf{x}_1)S_1(\mathbf{x}_2) + \frac{1}{2\pi}\int_0^{g(r)} \frac{dt}{\sqrt{1-t^2}} \times \exp\left(-\frac{\alpha(\mathbf{x}_1)^2 - 2\alpha(\mathbf{x}_1)\alpha(\mathbf{x}_2)t + \alpha(\mathbf{x}_2)^2}{2(1-t^2)}\right)dt \tag{2}$$

with $r=|\mathbf{x}_1-\mathbf{x}_2|$. Equation (2) was obtained from Eq. (A6) of Ref. [24]. Note that when $\alpha(\mathbf{x})$ is not a constant, the dependency of S_2 is explicitly on $\mathbf{x}_1$ and $\mathbf{x}_2$ and not only on their difference, as would be the case for statistically homogeneous morphologies.

The relation between the two-point function and the specific surface area was first derived by Debye in the case of a statistically homogeneous and isotropic morphology [25], and later generalized by Berryman to anisotropic yet statistically homogeneous morphologies [26]. The result of Berryman is further generalized to inhomogeneous morphologies in Ref. [40]: the average local surface area per unit volume $s(\mathbf{x})$ is

$$-\frac{s(\mathbf{x})}{4} = \frac{1}{4\pi}\int d\hat{\omega} \lim_{r\to 0}\frac{\partial S_2(\mathbf{x},\mathbf{x}+r\hat{\omega})}{\partial r}, \tag{3}$$

where $\hat{\omega}$ is a unit vector and the integral is over all directions of space. In the case of nonhomogeneously clipped GRF

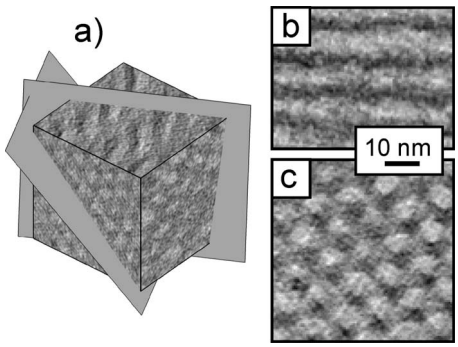

FIG. 3. Electron tomogram of SBA-15 mesoporous silica (a), and 2D slices of the reconstruction taken parallel (b) and orthogonal (c) to direction of the main channels.

with two-point function given by Eq. (2), this result becomes

$$s(\mathbf{x}) = \frac{4}{l_C}\frac{1}{\pi\sqrt{2}}\exp\left[-\frac{\alpha(\mathbf{x})^2}{2}\right]F\left(\frac{l_C|\nabla\alpha(\mathbf{x})|}{2}\right), \tag{4}$$

where l_C is the correlation length of the GRF, derived from the short-distance expansion of the field correlation function $g(r)\approx 1-(r/l_C)^2$. The function F in Eq. (4) is

$$F(x) = \frac{1}{2}\exp[-x^2] + \left(x+\frac{1}{2x}\right)\frac{\sqrt{\pi}}{2}\mathrm{erf}(x). \tag{5}$$

Calculations leading from Eqs. (2) and (3) to Eqs. (4) and (5) are straightforward yet lengthy; the details can be found in Ref. [40].

The total surface area of objects like those in Fig. 2 is obtained by integrating $s(\mathbf{x})$ over space. If $l_C|\nabla\alpha(\mathbf{x})|\ll 1$, Eq. (5) is approximated by $F\sim 1$ and Eq. (4) reduces to the specific surface area of homogeneously clipped GRF [e.g., [24]]. The other limit is $l_C|\nabla\alpha(\mathbf{x})|\gg 1$, i.e., when $\alpha(\mathbf{x})$ can be considered discontinuous over length scales comparable with l_C. In that case, Eq. (5) is approximated by $F\sim x\sqrt{\pi/2}$, which leads to $s(\mathbf{x})=|\nabla S_1(\mathbf{x})|$. The extra surface area resulting from the variation of α is the area of the surface of discontinuity multiplied by the jump in density across that surface. When neither approximation applies, the total surface area is obtained by integrating Eq. (4) over the entire volume of the material. For the rough interface in Figs. 1(c), with $|\nabla\alpha|$ equal to a constant, the integral can be calculated analytically. The roughness factor f_r defined as the ratio of total surface area to the geometric interface area [27], is found to be

$$f_r = \frac{4}{\sqrt{\pi}l_C|\nabla\alpha|}F\left(\frac{l_C|\nabla\alpha|}{2}\right). \tag{6}$$

In the particular case of Fig. 1(c), obtained with $l_C|\nabla\alpha(\mathbf{x})| = 1/2$, Eq. (6) predicts $f_r=4.6$.

The general results are now particularized to analyze the morphology of SBA-15 ordered mesoporous silica synthesized by liquid crystal templating [28]. SBA-15 has numerous applications, notably in catalysis [29], for the synthesis of nanoparticles [30], as well as for the study of confinement effects on physicochemical phenomena [31,32]. Figure 3(a)

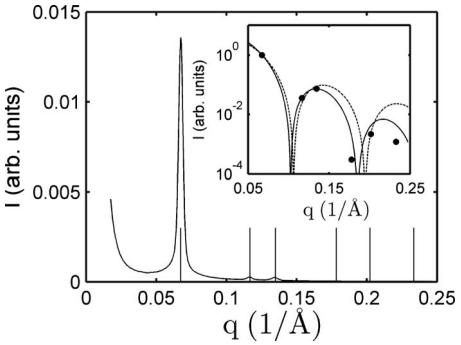

FIG. 4. SAXS pattern of SBA-15 in with vertical lines corresponding to a hexagonal lattice with spacing 10.8 nm. The intensity of the peaks is fitted in the inset with a cylindrical form factor (dashed line) and with the nonhomogeneously clipped GRF (solid line).

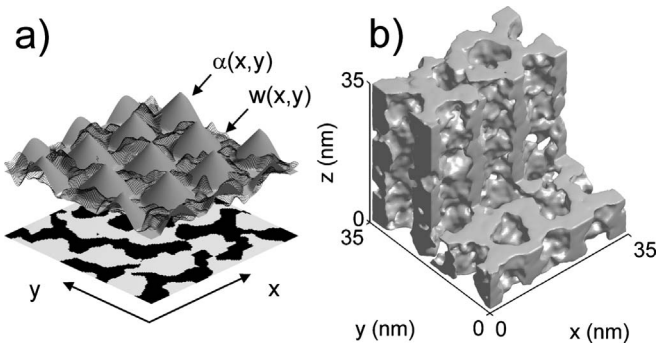

FIG. 5. Modeling of SBA-15 with $\alpha(\mathbf{x})$ being a 2D periodic function with hexagonal symmetry (a), and realization of the 3D model (b) with parameters derived from SAXS and nitrogen adsorption.

is an electron tomography reconstruction of SBA-15 [33,34], which provides a 3D map of the material with a nanometer resolution. The morphology of SBA-15 is approximated by a 2D hexagonal array of uniformly sized cylindrical pores [Figs. 3(b) and 3(c)] with diameter about 6 nm. The hexagonal symmetry is also detected in small-angle x-ray scattering (SAXS) measured on the same sample, which exhibits a series of diffraction peaks at characteristic angular positions [Fig. 4(a)], with a lattice parameter $a=10.8$ nm.

Nitrogen adsorption measurements done on the same sample yield a pore volume of 0.66 cm^3/g—of which 0.09 cm^3/g are due to molecular-sized micropores in the silica—and a surface area of 419 m^2/gm [33]. Using $\rho=2.2$ $g/.cm^3$ as the density of nonporous silica, the micropore volume leads to an effective density of 1.84 g/cm^3. Using the latter value, and estimating the area of a hexagonal unit cell as $\sqrt{3}a^2/2$ with $a=10.8$ nm, the specific mesopore volume and area are converted to a pore volume V_L and pore surface area S_L per unit length of the main channels. The values are $V_L=51.5$ nm^2 and $S_L=38.0$ nm. These two values would correspond to cylindrical pores with diameter $d=8$ nm and $d=12$ nm, respectively. The difference between the two estimates points to a surface-to-volume ratio incompatible with simple cylindrical pores.

In addition to the irregular shape of the mesopores that is clear from electron tomography [Fig. 3(b)], there is also a so-called complementary porosity that connects laterally the main pores [35]. The latter porosity is a key determinant of the activity of heterogeneous catalysts supported on SBA-15 [29]: it increases the accessibility of the active sites to reactant molecules, and it is also expected to play a major role during the impregnation of SBA-15. The complementary porosity is also a key for understanding the nanomechanical properties of the material [32]. Although the existence of a complementary porosity has been repeatedly evidenced through indirect methods [35,36] it is largely beyond the resolution limit of electron tomography [33], and its characterization remains a challenge.

A complete morphological model of SBA-15, comprising both the main channels and the complementary porosity, is obtained by clipping a GRF with a function $\alpha(\mathbf{x})$ that is maximum in the center of the pores, and minimum in the region of the wall. This is illustrated in Fig. 5(a), with a clipping function given by

$$\alpha(x,y,z) = \alpha_0 + (\alpha_1 - \alpha_0)\sum_i \Delta[r = d_i(x,y)], \tag{7}$$

where the sum covers all nodes of a hexagonal lattice; $d_i(x,y)$ is the distance to the i^{th} node, and $\Delta(r)=(1-r/R)\Theta(R-r)$ with R a constant. The clipping function $\alpha(\mathbf{x})$ has a constant gradient $(\alpha_1-\alpha_0)/R$ close to the nodes, which accounts for an interface with tunable roughness according to Eq. (6). For $r>R$ the clipping level is α_0, which accounts for the complementary porosity, the latter being non existent in the limit $\alpha_0 \to -\infty$.

The total pore volume V_L per unit pore length is obtained by integrating $[1-S_1(\mathbf{x})]$ over a unit hexagonal cell. From Eq. (1) with $\alpha(\mathbf{x})$ given by Eq. (7), one finds

$$\begin{aligned} V_L = & \left[1 + \operatorname{erf}\left(\frac{\alpha_0}{\sqrt{2}}\right)\right]\frac{\sqrt{3}a^2}{4} \\ & + \frac{R^2\sqrt{\pi}}{(\alpha_1-\alpha_0)^2}\left\{(1+\alpha_1^2)\frac{\sqrt{\pi}}{2}\left[\operatorname{erf}\left(\frac{\alpha_1}{\sqrt{2}}\right) - \operatorname{erf}\left(\frac{\alpha_0}{\sqrt{2}}\right)\right]\right. \\ & + \frac{\alpha_1}{\sqrt{2}}\left[\exp\left(-\frac{\alpha_1^2}{2}\right) - \exp\left(-\frac{\alpha_0^2}{2}\right)\right] \\ & \left. + \frac{\alpha_0-\alpha_1}{\sqrt{2}}\exp\left(-\frac{\alpha_0^2}{2}\right)\right\}, \end{aligned} \tag{8}$$

where $\sqrt{3}a^2/2$ is the total area of the unit cell. Knowing $a=10.8$ nm from the angular position of the SAXS peaks (Fig. 4), Eq. (8) relates V_L to parameters α_0, α_1, and R of the model. In the following, Eq. (8) is used to impose the experimental value $V_L=51.5$ nm^2 obtained from nitrogen adsorption, while fitting the intensities of the SAXS peaks in Fig. 4.

The SAXS intensity of a biphasic structure is proportional to the Fourier transform of the so-called stick probability function $P(\mathbf{r})$ [37,38], defined as the probability that a stick with length $\mathbf{r}$ tossed randomly in the material has both ends within a given phase. For statistically homogeneous materi-

als, $P(\mathbf{r})$ coincides with the two-point probability function $S_2(\mathbf{r}=\mathbf{x}_1\text{-}\mathbf{x}_2)$. In general, however, $P(\mathbf{r})$ is obtained through a spatial averaging as

$$P(\mathbf{r}) = \frac{1}{V_x}\int_{V_x} S_2(\mathbf{x},\mathbf{x}+\mathbf{r})\mathrm{d}V_x, \tag{9}$$

where V_x is the volume of the material. The analysis of the background scattering in Fig. 4 would require combining Eq. (2) with Eq. (9), and evaluating a Fourier transform. The analysis of the peak intensities is much simpler because it only depends on long-ranged correlations. Over long distances, Eq. (2) reduces to $S(\mathbf{x}_1,\mathbf{x}_2)\approx S_1(\mathbf{x}_1)S_1(\mathbf{x}_2)$ because $g(r)\approx 0$, from which $P(\mathbf{r})$ is proportional to the self-convolution of $S_1(\mathbf{x})$ with itself. Therefore, the intensity of the SAXS peaks can be analyzed in the usual way using $|A(q)|^2$ as a form factor [39], with $A(q)$ being the Fourier transform of $S_1(\mathbf{x})$ within a single hexagonal cell. The shape of $A(q)$ is not modified if a constant is subtracted from $S_1(\mathbf{x})$; subtracting $[1-\mathrm{erf}(\alpha_0/\sqrt{2})]/2$ from Eq. (1) leads to

$$A(q) = \int_0^R J_0(qr)\frac{1}{2}\left\{\mathrm{erf}\left(\frac{\alpha(\mathrm{r})}{\sqrt{2}}\right) - \mathrm{erf}\left(\frac{\alpha_0}{\sqrt{2}}\right)\right\} rdr, \tag{10}$$

where $\alpha(r)=\alpha_0+(\alpha_1-\alpha_0)\Delta(r)$. The solid line in the inset of Fig. 4 is the least-square fit of the peak intensities with Eq. (10), with only α_0 and α_1 as adjustable parameters. The value of parameter R is obtained through Eq. (8) with $V_\mathrm{L}=51.5$ nm^2, for any value of α_0 and α_1. The fitted values are $\alpha_0=-1.08$, $\alpha_1=5.27$, and $R=4.65$ nm. It should be noted that R is smaller than half the hexagonal lattice size, so there is indeed a region with constant $\alpha(\mathrm{x})=\alpha_0$ between neighboring pores. The hexagonal symmetry of the clipping function has therefore no effect of the shape of the pore sections which are found to be statistically isotropic.

The correlation length of the GRF cannot be identified from the peak intensities because l_C does not appear in Eqs. (8) and (10). The characteristic length can be obtained from the experimental specific surface area per unit length of the channels, $S_\mathrm{L}=38.0$ nm. In the context of our model, S_L is obtained by integrating Eq. (4) over a unit hexagonal cell. Noting that the gradient of $\alpha(\mathbf{x})$ is a constant for distances to the center shorter than R and that it vanishes elsewhere, the following analytical result is obtained

$$S_\mathrm{L} = \frac{4}{l_C\pi\sqrt{2}}\left\{\left(\frac{\sqrt{3}a^2}{2}-\pi R^2\right)\exp\left(-\frac{\alpha_0^2}{2}\right) + \frac{2\pi R^2}{(\alpha_0-\alpha_1)^2}F\left[\frac{l_C(\alpha_1-\alpha_0)}{2R}\right]\left\{\alpha_1\sqrt{\frac{\pi}{2}}\left[\mathrm{erf}\left(\frac{\alpha_1}{\sqrt{2}}\right) - \mathrm{erf}\left(\frac{\alpha_0}{\sqrt{2}}\right)\right] - \left[\exp\left(-\frac{\alpha_0^2}{2}\right)-\exp\left(-\frac{\alpha_1^2}{2}\right)\right]\right\}\right\} \tag{11}$$

in which all parameters are known but l_C. Equating S_L to 38 nm and solving Eq. (11) numerically leads to $l_C=1.6$ nm.

Figure 5(b) was obtained with a GRF having $g(r)=1/\cosh(r/\xi)$ with $\xi=1.14$ nm, corresponding to $l_C=1.6$ nm, and other parameters derived previously from SAXS and nitrogen adsorption. With simple morphological models, it is mostly through incoherencies between SAXS and adsorption analyses that the existence of the complementary porosity is acknowledged [e.g., [33]]. The use of a non-homogeneously clipped GRF enables us to analyze coherently SAXS and adsorption within a single morphological model. This leads to a description of the complementary porosity which is crucial for applications of SBA-15, notably in catalysis.

C.J.G. acknowledges support from the National Funds for Scientific Research (F.R.S.-FNRS, Belgium). The authors are obliged to M. Wolters for synthesizing the SBA-15 sample, to H. Friedrich for the electron tomography, and to P. E. de Jongh and K. P. de Jong for helpful suggestions.

[1] G. Matheron, *Elements Pour Une Théorie des Milieux Poreux* (Masson, Paris, 1967).
[2] S. Torquato, *Random Heterogeneous Materials: Microstructure and Macroscopic Properties* (Springer, New York, 2001).
[3] A. P. Roberts and E. J. Garboczi, Proc. R. Soc. London, Ser. A **458**, 1033 (2002).
[4] C. H. Arns, M. A. Knackstedt, and K. R. Mecke, Phys. Rev. Lett. **91**, 215506 (2003).
[5] E. Roduner, Chem. Soc. Rev. **35**, 583 (2006).
[6] J. W. Cahn, J. Chem. Phys. **42**, 93 (1965).
[7] J. A. Quiblier, J. Colloid Interface Sci. **98**, 84 (1984).
[8] N. F. Berk, Phys. Rev. Lett. **58**, 2718 (1987).
[9] M. Teubner and R. Strey, J. Chem. Phys. **87**, 3195 (1987).
[10] N. F. Berk, Phys. Rev. A **44**, 5069 (1991).
[11] S. H. Chen, D. D. Lee, K. Kimishima, H. Jinnai, and T. Hashimoto, Phys. Rev. E **54**, 6526 (1996).
[12] F. Bron and D. Jeulin, Image Anal. Stereol. **23**, 33 (2004).
[13] P. Levitz, Adv. Colloid Interface Sci. **76-77**, 71 (1998).
[14] A. P. Roberts, Phys. Rev. E **55**, R1286 (1997).
[15] C. J. Gommes and A. P. Roberts, Phys. Rev. E **77**, 041409 (2008).
[16] A. P. Roberts, Phys. Rev. E **56**, 3203 (1997).
[17] D. J. Nott and R. J. Wilson, Signal Process. **80**, 125 (2000).
[18] V. De Oliveira, Comput. Stat. Data Anal. **34**, 299 (2000).
[19] J. A. Quintanilla and W. M. Jones, Phys. Rev. E **75**, 046709 (2007).
[20] M. Grigoriu, J. Appl. Phys. **94**, 3762 (2003).
[21] Y. Yin and A. P. Alivisatos, Nature (London) **437**, 664 (2005).
[22] I. W. Hamley, Angew. Chem., Int. Ed. **42**, 1692 (2003).
[23] J. Quintanilla and S. Torquato, Phys. Rev. E **55**, 1558 (1997).
[24] A. P. Roberts and M. A. Knackstedt, Phys. Rev. E **54**, 2313 (1996).
[25] P. Debye, H. R. Anderson, and H. Brumberger, J. Appl. Phys. **28**, 679 (1957).
[26] J. G. Berryman, J. Math. Phys. **28**, 244 (1987).
[27] A. D. McNaught, and A. Wilkinson, *Compendium of Chemical*

Terminology (Blackwell Scientific, Oxford, 1997).
[28] D. Zhao, J. Feng, Q. Huo, N. Melosh, G. H. Fredrickson, B. F. Chmelka, and G. D. Stucky, Science **279**, 548 (1998).
[29] J. R. A. Sietsma, J. D. Meeldijk, J. P. den Breejen, M. Versluijs-Helder, A. J van Dillen, P. E. de Jongh, and K. P. de Jong, Angew. Chem., Int. Ed. **46**, 4547 (2007).
[30] F. Gao, Q. Lu, X. Liu, Y. Yan, and D. Zhao, Nano Lett. **1**, 743 (2001).
[31] G. Dosseh, X. Yongde, and C. Alba-Simionesco, J. Phys. Chem. B **107**, 6445 (2003).
[32] J. Prass, D. Müter, P. Fratzl, and O. Paris, Appl. Phys. Lett. **95**, 083121 (2009).
[33] C. J. Gommes, H. Friedrich, M. Wolters, P. E. de Jongh, and K. P. de Jong, Chem. Mater. **21**, 1311 (2009).
[34] H. Friedrich, P. E. de Jongh, A. J. Verkleij, and K. P. de Jong, Chem. Rev. (Washington, D.C.) **109**, 1613 (2009).
[35] M. Kruk, M. Jaroniec, C. H. Ko, and R. Ryoo, Chem. Mater. **12**, 1961 (2000).
[36] Z. Liu, O. Terasaki, T. Ohsuna, K. Hiraga, H. J. Shin, and R. Ryoo, ChemPhysChem **2**, 229 (2001).
[37] S. Ciccariello, G. Cocco, A. Benedetti, and S. Enzo, Phys. Rev. B **23**, 6474 (1981).
[38] O. Glatter and K. Kratky, *Small-Angle X-ray Scattering* (Academic, London, 1982).
[39] S. Förster, A. Timmann, M. Konrad, C. Schellbach, A. Meyer, S. S. Funari, P. Mulvaney, and R. Knott, J. Phys. Chem. B **109**, 1347 (2005).
[40] See EPAPS Document No. E-PLEEE8-80-014912for the derivation of the relation between 2–point function and specific surface area for inhomogeneous morphologies, as well as for the details of calculations leading to Eq. (4). For more information on EPAPS, see http://www.aip.org/pubservs/epaps.html.